A BELLEVILLE-SPRING BASED ELECTROMAGNETIC ENERGY HARVESTER

Davide Castagnetti

Department of Engineering Sciences and Methods,

University of Modena and Reggio Emilia

42122 - Reggio Emilia (RE), Italy

Email: davide.castagnetti@unimore.it

Keywords

Energy harvesting, Belleville spring, large bandwidth, electromagnetic, experimental, piezoelectric, hybrid converter.

ABSTRACT

Energy harvesting from kinetic ambient energy is particularly effective to power autonomous sensors. This work proposes an innovative energy converter based on two counteracting Belleville springs and exploiting their peculiarity, for a height to thickness ratio equal to 1.414, of nearly zero stiffness over a wide deflection range. After analytical and numerical modelling a prototype is developed and experimentally investigated. The sub-optimal geometry of the commercial springs used in the prototype, together with a non-ideal response makes the operating frequency for the prototype higher than analytical and numerical predictions. Nevertheless, the harvester exhibits a significantly large bandwidth, together with a high output power, compared to similar solutions in the literature, for all the examined configurations and input excitations.

INTRODUCTION

The work deals with the development of an innovative energy harvester exploiting Belleville springs. Kinetic ambient energy, which is the most common source for energy harvesting, usually occurs in the form of vibrations or random forces, being intrinsically frequency-variant in a low frequency range [1]-[6]. Therefore, it is challenging to develop energy harvesting systems able to efficiently harvest energy in the low frequency range and with a large bandwidth. Among the available conversion techniques, electromagnetic and piezoelectric are surely the most promising in terms of simplicity, output current and voltage [4]-[5]. Many harvesters either relying on electromagnetic [7]-[17] or on piezoelectric [18]-[35] technique have been presented in the literature. In particular, energy harvesters can have either a linear [18]-[31] or non-linear [32]-[55] response. Among non-linear energy harvesters, particular interest deserve those using Duffing oscillators [36]-[55], which have the peculiar feature of a broadband response. Some hybrid harvesters have been proposed in addition, combining piezoelectric and electromagnetic technology [56]-[57].

Two are the limits of many solutions proposed in the literature: first, their relatively high operating frequency; second, a low quality factor, i.e. the typically high conversion efficiency of the harvester abruptly decreases as the excitation frequency does not match the system eigenfrequency. In case of electromagnetic harvesters, the operating frequency usually falls in the range from 10 Hz to 100 Hz, while in case of piezoelectric harvesters, apart from few exceptions [23], [29]-[31], it is typically in the range from 50 Hz to 300 Hz.

This work aims to overcome these limitations by proposing an innovative electromagnetic energy converter operating over a large bandwidth. This new solution is based on two counteracting Belleville springs and exploits their peculiarity, for a height to thickness ratio equal to 1.414, of nearly zero stiffness over a wide deflection range.

The paper is organized into four steps. In the first step we introduce the force-displacement characteristic of Belleville springs and some engineering applications. In the second step, we propose and examine a conceptual solution for an energy harvester relying on Belleville springs. The innovative nature of the solution is its simple and compact structure, which can be organized either in series or parallel in order to improve the output power or achieve a multi-frequency behaviour. In the third step, the harvester is modelled analytically. The fourth step presents the prototype development and experimental validation of the harvester.

The experimental assessment on the prototype, which was manufactured using off the shelf springs, highlights a remarkably large bandwidth of the harvester, together with high conversion efficiency, also in comparison with similar solutions reported in the literature [58] or commercial products [59]. By contrast, due to secondary effects, the operating frequencies are higher than expected from analytical and numerical predictions. Compared to non-linear energy harvesters presented in the literature, and in particular to those relying on Duffing oscillators [36]-[55], the proposed solution is quite simple and innovative. The elastic system featuring two counteracting Belleville springs can have either a linear or a non-linear and bi-stable response depending on the preload applied to the springs. The harvester can include either electromagnetic or piezoelectric transduction but also a hybrid of both, thus enhancing efficient energy conversion.

1. BELLEVILLE SPRINGS RESPONSE AND APPLICATIONS

Patented by J. F. Belleville in 1867, Belleville springs (Figure 1) are coned disk springs which have been extensively used in many engineering applications, due to their peculiar characteristics. Belleville springs are compact along the loading axis, enable to obtain a wide variety of load-deflection characteristics by simply changing geometric proportions, and provide the possibility to vary the load-capacity and deflection range by using multiple springs in series and/or parallel. Some examples of applications in industrial and machine constructions are spring suspensions, valves actuation, overload and slip clutches (to achieve the desired preload between friction discs), holding brake, backlash compensation, and in general applications involving energy storage or, more recently, impact energy dissipation [60]-[61].

An accurate analytical model for Belleville springs was proposed by Almen and Laszlo [62], which provided formulas for stresses and displacements calculation. According to this analytical model, the force-deflection relation of a Belleville spring (Figure 1) is given by the following formula:

$$P = 4K\frac{E\,s^4}{D^2}\eta \tag{1}$$

where E is the Young's modulus of the material, s represents the spring thickness, D the outer spring diameter, K is defined as:

$$K = \pi\left(\frac{c}{c-1}\right)^2\left(\frac{c+1}{c-1}-\frac{2}{\ln c}\right) \tag{2}$$

being c the ratio between the outer and inner diameter of the spring (= D / d), and finally η is defined by the following formula:

$$\eta = \frac{1}{1-\nu^2}\frac{f}{s}\left[\left(\frac{h}{s}-\frac{f}{s}\right)\left(\frac{h}{s}-\frac{1}{2}\frac{f}{s}\right)+1\right] \tag{3}$$

In the above formula, ν is the Poisson's ratio of the spring material, f is the axial deflection of the spring, and h is the free height of the conical spring measured as the elevation of the truncated cone formed by either the upper or lower surface (Figure 1). By assuming P_0 as the load which flattens the conical spring producing a deflection f = h, equation (1) yields the following dimensionless relationship between load and deflection:

$$\frac{P}{P_0} = \frac{f}{h}\left[\left(\frac{h}{s}\right)^2\left(1-\frac{f}{h}\right)\left(1-\frac{1}{2}\frac{f}{s}\right)+1\right] \tag{4}$$

The above relationship highlights that the spring rate of a Belleville spring can be easily varied over a wide range by simply changing the height to thickness ratio (h/s) of the conical disc.

The normalized force-deflection curves in Figure 2 show to which extent the characteristic of a Belleville spring can vary from linear to largely non-linear by increasing the height to thickness ratio from 0 up to 2. The curves corresponding to a low height to thickness ratio are approximately linear. For a ratio h/s = 1.414 (dashed line in Figure 2) the curve shows a nearly constant load for a deflection range which extends symmetrically across the flat position, from a ratio f/h ranging from about 0.6 up to 1.4. This almost zero stiffness across the flat position can be usefully exploited to develop structures for energy harvesters. Values of the height to thickness ratio higher than 1.414 provide highly non-linear curves (Figure 2), where the load reaches a local maximum and minimum respectively before and after the flat position.

2. CONCEPTUAL HARVESTER SOLUTIONS

Figure 3 shows the conceptual solution of an energy harvester exploiting Belleville springs. Two counteracting Belleville springs ($B1$ and $B2$), having the base of the cone on the outer side, are enclosed into an external tubular frame (F), and separated by a tubular spacer (S) interposed in between. By means of a couple of tubular fixtures (R), exactly fitting into the frame (F), the Belleville springs are preloaded up to their flat configuration. According to the curves in Figure 2, for an h/s ratio of the Belleville springs equal to 1.414, this elastic system features nearly zero stiffness up to a stroke (on each side of the equilibrium configuration) nearly equal to 20% of the height h of the coned spring.

Through the axial rod (T) supported by the Belleville springs ($B1$ and $B2$), we obtain a simple one-degree of freedom mechanism, which can be exploited both for electromagnetic and piezoelectric energy harvesting (Figure 3). On the one hand, a simple electromagnetic energy harvester can be obtained by applying a permanent magnet (M) to each end of the sliding rod (T) and enclosing each magnet in a coil (C). The oscillation of the elastic system across the equilibrium configuration originates a relative translation between the magnets and the coils, thus converting kinetic energy into output voltage at the ends of the coils. On the other hand, the system can include also a simple piezoelectric converter obtained by bonding piezoelectric patches (P) to the surface of the Belleville springs. As the springs deform due to dynamic excitation of the system, the strained piezoelectric patches provide an output voltage on their opposite surfaces.

By combining these solutions we have a hybrid electromagnetic and piezoelectric harvester, featuring a symmetric configuration with respect to the cross mid-plane of the structure.

3. ANALYTICAL MODEL OF THE HARVESTER

3.1. Elastic response

Assuming an elastic behaviour of the Belleville springs, Figure 4 shows the model of the equivalent mass-springs system corresponding to the converter in Figure 3. Differently from Figure 3, in order to be able to describe a more general configuration, the equivalent mass-spring system in Figure 4 is vertically oriented. This configuration, which can occur in practice depending on the set-up of the system, allows to takes into account the weight load of the suspended mass, due to gravity (g).

The total force on the sliding rod (T) comes from two different contributions: i) the sum of the opposite elastic forces exerted by each of the counteracting Belleville springs, which are provided by equation (1); ii) the weight load of the rod itself, acting downward. It comes that, in the equilibrium configuration, the Belleville springs have a different deflection f, summing up two contributions: i) a deflection equal to their free height h, due to preload; ii) a deflection Δ due to the weight load of the oscillating mass, which increases the deflection of the bottom spring ($B1$), while decreasing that of the top spring ($B2$). Therefore, the resulting deflection f for Belleville springs $B1$ and $B2$ respectively is given by:

$$f_{B1} = h - u + \Delta \tag{5}$$

$$f_{B2} = h + u - \Delta \tag{6}$$

From equation (1) the expression of the elastic force is:

$$P = 4K\frac{E\,s^4}{D^2}\left(\eta_{B1} - \eta_{B2}\right) \tag{7}$$

where η_{B1} and η_{B2} refer to the Belleville springs $B1$ and $B2$ respectively, and according to equation (3), (5) and (6) their expression is:

$$\eta_{B1} = \frac{1}{1-\nu^2}\frac{h-u+\Delta}{s}\left[\left(\frac{h}{s}-\frac{h-u+\Delta}{s}\right)\left(\frac{h}{s}-\frac{1}{2}\frac{h-u+\Delta}{s}\right)+1\right] \quad (8)$$

$$\eta_{B2} = \frac{1}{1-\nu^2}\frac{h+u-\Delta}{s}\left[\left(\frac{h}{s}-\frac{h+u-\Delta}{s}\right)\left(\frac{h}{s}-\frac{1}{2}\frac{h+u-\Delta}{s}\right)+1\right] \quad (9)$$

By replacing equation (8) and (9) into equation (7) and rearranging the terms, the following expression of the total elastic force on the sliding rod (T) is obtained:

$$P = \frac{4KEs}{D^2(1-\nu^2)}\left(-(h^2-2s^2-\Delta^2)\Delta+(h^2-2s^2-3\Delta^2)u+3\Delta u^2-u^3\right) \quad (10)$$

Equation (10) highlights that the elastic force on the rod (T): (i) is strongly non-linear with the displacement, (ii) due to weight load it acts downward when the rod is in the central equilibrium position (u = 0), and (iii) increases in modulus as the stroke u of the rod increases.

3.2. Fundamental eigenfrequency

The fundamental eigenfrequency of the system can be found from the differential equation of motion [63], which governs the free motion of the undamped system. By equalling the inertial forces to the elastic ones (equation (10)) we have the following expression:

$$m\ddot{u}(t)+\frac{4KEs}{D^2(1-\nu^2)}\left(-(h^2-2s^2-\Delta^2)\Delta+(h^2-2s^2-3\Delta^2)u(t)+3\Delta u^2(t)-u^3(t)\right) \quad (11)$$

where m is the mass of the rod (T). Equation (11) is a second order differential equation from which the first derivative is absent, and it does not have a closed-form solution. In case either the weight load is negligible or the system is oriented horizontally (thus Δ = 0), this equation reduces to the following form:

$$m\ddot{u}(t)+\frac{4KEs}{D^2\left(1-\nu^2\right)}\left(\left(h^2-2s^2\right)u(t)-u^3(t)\right)=0 \tag{12}$$

which, according to [64], can be simply reduced to the following dimensionless form, known as Duffing equation:

$$\ddot{u}^*(t)+u^*(t)+\varepsilon u^{*3}(t)=0 \tag{13}$$

where u^* is the dimensionless displacement and ε is a dimensionless parameter which measures the strength of the nonlinearity. According to the exact solution proposed in [64], the fundamental circular frequency ω of equation (8) is a function of the degree of nonlinearity ε.

For small displacements across the equilibrium configuration in Figure 3, the non-linear (cubic) term of equation (12) can be neglected, giving the following simplified linear equation of motion:

$$m\ddot{u}(t)+\alpha u(t)=0 \tag{14}$$

where:

$$\alpha=\frac{4KEs\left(h^2-2s^2\right)}{D^2\left(1-\nu^2\right)} \tag{15}$$

By assuming a harmonic and symmetric dynamic excitation applied to the system ($u(t)=u_0\sin(\omega t)$), equation (14) provides the fundamental circular frequency ω:

$$\omega = \frac{2}{D}\sqrt{\frac{KEs\left(2s^2 - h^2\right)}{m\left(1-\nu^2\right)}} \tag{16}$$

Accordingly, equation (16) yields the fundamental frequency f_0 , which is equal to:

$$f_0 = \frac{1}{\pi D}\sqrt{\frac{KEs\left(2s^2 - h^2\right)}{m\left(1-\nu^2\right)}} \tag{17}$$

3.3. Output power

According to Williams and Yates [65], the maximum power that this device can generate is given by:

$$P_{\max} = m\zeta_t f_n^3 Z_{\max}^2 \tag{18}$$

where m is the mass of the oscillating equipment (rod and permanent magnets), ζ_t is the damping ratio, f_n is the resonant frequency of the harvester, and Z_{max} is the maximum relative displacement between the coil and the permanent magnet (Figure 3).

3.4. Case study

To provide an example of the system peculiar features, we assume to use a Belleville spring, with outer diameter D equal to 50 mm, inner diameter d equal to 20 mm, thickness s equal to 0.5 mm, and height h equal to 0.707, so as to match exactly the desired height to thickness ratio of 1.414. In addition, we consider a steel rod, having a diameter of 20 mm and 40 mm long, rigidly connected to the Belleville springs.

Figure 5 shows the absolute load value acting on the rod by the counteracting Belleville springs as a function of the rod stroke. The curve highlights the stable equilibrium position for the device in its centre configuration and the relatively wide displacement range (about 25% of the stroke) characterized by a nearly zero stiffness. According to the simplified equation (17), the eigenfrequency of this elastic system results equal to 4.35 Hz, thus being very low.

On the basis of these encouraging results, the following section presents the development and assessment of a prototype, to provide experimental validation of the concept.

4. HARVESTER PROTOTYPE DEVELOPMENT

This section presents the development of the harvester prototype with regard to Belleville springs selection and characterization, system design and finite element (FE) simulation. The use of commercial components for the development of the prototype was the main guideline in the design of the energy harvester.

4.1. Belleville springs selection

The selection of the Belleville springs for the prototype involved two main criteria: (i) a height to thickness ratio h/s equal to 1.414, (ii) commercially available springs.

A research on commercially available Belleville springs pointed out the unavailability of off the shelf springs having a height to thickness ratio h/s exactly equal to 1.414, and dimensions close to the tentative values proposed in the previous section example, which would allow to build a small prototype.

Table 1 reports the dimensions of two commercially available Belleville springs that were initially taken into account. These springs are made of C75S cold rolled steel with a Young's modulus of 206 GPa, a Poisson's ratio of 0.3, a tensile strength equal to 1170 MPa (at a 15% elongation). The force-deflection response of these two springs was experimentally investigated through quasi-static compression tests performed using conical fixtures.

Finally, spring #1 in Table 1 was chosen since, as shown in Figure 6, it provided a force-deflection response quite close to the requirements, as expected from the h/s ratio. However, three main discrepancies appear between the experimental measurement (dashed line in Figure 6) and the analytical prediction (solid line in Figure 6). First, a slightly lower stiffness of the spring compared to the analytical prediction. This may be imputed to the measurement through the displacement transducer on the tensometer, which is installed far from the specimens, thus including the compliances of the whole kinematic chain of the machine. Second, a small hysteresis between the loading and unloading curve, which is caused both by friction between the spring and the fixtures and by plastic strains that locally occurs in the spring cross section (see

Results section). Third, since the value of the h/s ratio is not the optimum one, the stiffness is slightly negative in the central part of the curve, giving a bi-stable behaviour.

4.2. Harvester prototype

The energy harvester prototype was designed on the basis of the commercial Belleville spring chosen in the previous step (Section 4.1). Accordingly, the dimensions of the elastic system and of the electromechanical converter relate directly to the diameter of the Belleville springs, in order to obtain a compact harvester and to allow a simple assembly and calibration of the system.

Figure 7 shows the technical drawing of the energy harvester prototype that was inspired by the conceptual solution in Figure 3. Compared to that configuration, the present architecture is slightly different, in order to simplify the assembly and make easier the tests on the prototype. First of all, the prototype in Figure 7 has a vertical axis, in order to allow a simple set-up on the electromagnetic shaker available in the laboratory. In addition, the prototype is not symmetric, with respect to the cross mid-plane of the mechanical system: the energy converter is on the top. Finally, only electromagnetic conversion was implemented in this first prototype, since the Belleville springs are quite small in the radial direction, so there is not enough room for piezoelectric patches. The counteracting Belleville springs (1), corresponding to #1 in Table 1, are supported between the male and the female part of commercial spherical washers (2) having an appropriate diameter. These spherical washers ensure a uniform contact both with the upper and lower base of the Belleville spring for the whole device stroke; in addition, they allow an easy assembly and enhance auto-alignment of the system when preload is applied. A tubular rod (3), acting as the spacer (S) in Figure 3, is interposed between the Belleville springs. This elastic system is assembled and preloaded through four angularly equispaced M5 bolt-nut fasteners, acting on the outer spherical washers. An additional M5 bolt (4), equivalent to the rod (T) in Figure 3, is rigidly connected to the axis of the tubular rod (3): this element transfers the dynamic excitation received by the oscillating mass of the system (spherical washers

(2) plus tubular rod (3)) to the electromagnetic conversion unit of the prototype (on the top).

The electromagnetic conversion was implemented using a NdFeB flat disc magnet (5) 35 mm in diameter and 5 mm thick (S35-05-N42 from Supermagnete [66]). The magnet is bonded to a nylon insert (6) which is screw fixed to the axial bolt (4). This nylon insert shields the magnetic field toward the metal core of the mechanical system, thus avoiding negative interactions, which could lower the performance of the system. A commercial PVC pipe (7) with an inner diameter equal to 36 mm was bonded to the frame top washer, and used to enclose the magnet (5) and support the copper coils (8). The whole system can be easily assembled, calibrated and fixed to a vibrating table for the tests. In addition, the electromagnetic conversion device can be simply equipped with additional magnets or the number of coils increased.

5. HARVESTER PROTOTYPE SIMULATION AND RESULTS

The FE modelling of the harvester prototype involves two steps. The first step evaluates the modal response of the converter prototype and the stress field in the Belleville springs, respectively through a mass-spring model and an axisymmetric model. The second analysis step investigates the electromagnetic converter through an axisymmetric magnetostatic model.

5.1. Mass-spring finite element model

Figure 8a shows the mass-spring FE model which describes the oscillating equipment (tubular rod (3), female part of the spherical washers (2), M5 axial bolt (4), magnet (5) and Teflon insert (6) in Figure 7) as a plane rigid body of equal mass (about 250 g). To reproduce the Belleville springs, the model includes two counteracting non-linear spring connectors which link the plane rigid body to the ground. The force-displacement characteristic of these connectors was defined according to equation (1), assuming the Belleville spring dimensions reported in Table 1. Built in constraints applied to the free end of each spring reproduce connection to the ground.

The analysis involves five static and one modal analysis steps. In order to preload the system to its equilibrium configuration, the first static analysis step compresses each free end of the springs of a quantity equal to the Belleville spring free height h. The subsequent four static analysis steps move the spring-supported mass from its central equilibrium configuration to the displacement value h, 0, -h and again 0 respectively, in order to describe a whole load cycle. The final modal analysis step, where the rod is free to oscillate across its central equilibrium configuration, involves the Lanczos algorithm. The FE model was implemented through the standard options of the ABAQUS/Standard package (version 6.12-3) [68].

5.2. Axisymmetric finite element model

Figure 8b shows the axisymmetric FE model of the harvester prototype which reproduces the Belleville springs ($B1$ and $B2$) through solid axisymmetric elements

(CAX4R [68]), while the inner oscillating mass (T) and the outer parts of the support spherical washers (W) are described as axisymmetric analytical rigid surfaces. For the Belleville springs, the linearly-elastic Hooke model described the behaviour of C75S cold rolled steel up to the yield stress S_y , which was assumed equal to 0.75 times the ultimate tensile strength S_u. The post-yield behaviour was described by a classical metal plasticity model, which uses a Mises yield surface. The yield strength, independent of the hydrostatic stress component, was defined as a function of the equivalent plastic strain.

Frictionless contact was enforced between the Belleville springs and their counterparts (the oscillating mass and the top and bottom conical supports).

The analysis involved the same five static analysis steps as in the mass-spring FE model defined in the previous section. Similarly, the FE model was implemented through the standard options of the ABAQUS/Standard package (version 6.12-3) [68].

5.3. Electromagnetic finite element modelling

Figure 8c shows the axisymmetric magnetostatic FE model of the harvester prototype. The model, which is focused on the electromagnetic converter, describes a spherical region of the system having its centre on the permanent magnet, up to a radius equal to three times that of the PVC pipe. Thus, in addition to the permanent magnet, also the PVC pipe, the coil, and part of the mechanical conversion device are included. Therefore the model provides both a detailed analysis of the electromagnetic conversion system and its interaction with the mechanical part of the converter.

A linear response described the permanent magnet material, with a maximum energy product equal to 40 MGOe (according to the data from the manufacturer [66]). A copper wire 0.2 mm in diameter was used for the coils. The PVC pipe, the Teflon insert, and air were described with the same linear properties since they have nearly the same relative permeability. A nonlinear soft magnetic material property described the steel components of the mechanical part of the converter. Asymptotic boundary conditions were applied on the sphere surface.

The mesh involved 5929 nodes and 11459 triangular elements. This model was implemented through the free Femm 4.2 software [67].

5.4. Results from the analytical and finite element simulation

Figure 10 shows the load-stroke curves of the rod (T) provided by the analytical model (solid black line), by the mass-spring FE model (empty red squares), and by the axisymmetric FE model (empty blue circles) for the harvester prototype in Figure 7, which involves the Belleville spring #1 in Table 1.

The fundamental frequency retrieved from the simplified analytical model (equation (17)) is equal to 6.03 Hz, while that from the mass-spring FE model is equal to 6.00 Hz. Figure 11 shows the Von Mises equivalent stress in the Belleville springs, deformed up to $h/2$ beyond their flat configuration. The close-up view highlights in grey the region where the stresses overcome the yield stress of the material (about 877 MPa).

Figure 12 displays the contour map of the flux of the magnetic field B in the converter and a close-up view of the interaction between the permanent magnet and the coil.

6. EXPERIMENTAL VALIDATION

Figure 9 shows the prototype of the energy harvester which was experimentally validated. Through an accurate calibration of the preload on the counteracting Belleville springs the harvester was set up in the central equilibrium configuration.

The experimental validation involved two steps. First, a quasi-static force-stroke characterization of the energy harvester. Second, the assessment of the modal response and of the output power of the energy harvester over a frequency range, from about 0 Hz up to 250 Hz, in order to obtain a comprehensive characterization of the dynamic response. The electromagnetic converter involved a 1000 coils configuration and three levels of permanent magnets: one, two and four, in order to clearly assess their effect on the output power. Since the coils resistance amounts to about 70 Ω, the following five resistive loads were examined: 68 Ω, 82 Ω, 100 Ω, 180 Ω, and open circuit. To assess the effect of the input acceleration on the system, two levels were investigated: 9.81 m/s^2 and 19.62 m/s^2.

6.1. Test set-up

The quasi-static force-stroke characterization of the converter involved only the frame of the converter implementing the elastic system. By fixing the frame of the converter, a quasi-static motion law (1 mm/s) was applied to the M5 axial bolt (5 in Figure 7) in order to reproduce the same cycle as in the FE simulation (0, h, 0, -h, 0). The test was performed through an electromechanical testing machine (Galdabini SUN 500).

All the experimental tests aimed at assessing the modal response of the harvester were performed through an electro-dynamic shaker (Data Physics BV400 [69]). In order to implement a closed-loop control on the system, a miniature accelerometer (MMF KS94B100 [70]) was applied to the vibrating table of the shaker. An identical accelerometer was fixed to the oscillating mass of the converter (Figure 9), in order to seek the eigenfrequencies of the system. The shaker was managed by an 8-channel Abacus controller and the whole testing apparatus was controlled by the Signal Star software, installed on a PC that was also used for data acquisition.

A 16-channel data acquisition module (USB 6251 from National Instruments [71]) registered the output voltage on the coil ends of the harvester prototype. The data acquisition module was managed by a notebook, equipped with the Labview SignalExpress software [72].

6.2. Results of the experimental validation

Figure 10 shows the load-stroke curve of the rod (T) measured experimentally (dashed black line) on the harvester prototype in Figure 7.

For a 100 Ω resistive load, Figure 13 displays the ratio of the output acceleration on the moving mass over the input acceleration on the frame, as a function of the excitation frequency. The diagrams are organized according to the input acceleration (9.81 m/s^2 on the left column, and 19.62 m/s^2 on the right column), and to the number of magnets (1 in the first row, 2 in the second row, and 4 in the bottom row).

With the same layout, Figure 14 shows the diagrams of the output voltage from the converter as a function of the exciting frequency.

Table 2 reports the peak output voltage and the corresponding peak output power registered experimentally for the harvester with 1 magnet, as a function of the resistive load level and of the input acceleration.

Similarly, Table 3 gives the experimental peak output voltage and power for the harvester with 2 and 4 magnets respectively, considering two input acceleration levels and a 100 Ω resistive load. The values in both tables refer to an input excitation tuned on the resonant frequency.

For a 100 Ω resistive load and two input acceleration levels, Figure 15 clearly compares the peak output voltage (Figure 15a) and the peak output power (Figure 15b) for different configurations of the harvesters in terms of number of magnets. Regarding the peak output power, the experimental results (white and blue column) are compared to the analytical prediction (dotted column) given by equation (18) presented in Section 3.3.

7. DISCUSSION

The load-stroke curves in Figure 10 highlight a quite close agreement between the analytical and FE prediction, in particular for the mass-spring FE model. The curves exhibit a nearly zero stiffness of the harvester across the central equilibrium position (Belleville springs deformed at flat position), since the Belleville springs reciprocally counteract each other. The prediction provided by the axisymmetric FE model, in the range from $-h/2$ to $h/2$, slightly differs from the analytical model and mass-spring FE model predictions. This disagreement can be imputed to a slightly different constraining of the spring in the axisymmetric FE model compared to the analytical model. A remarkably different response was registered experimentally. First, the converter prototype provides a significantly lower load than analytical prediction towards the ends of the loading cycle. Second, across the central equilibrium position the experimental response exhibit a non-monotonic behaviour with two local maxima and a negative stiffness in-between. This peculiar response fully complies with that from the single Belleville spring (Figure 6) and highlights a bi-stable response of the system.

According to the analytical and mass-spring FE model, the fundamental frequency of the converter is quite low, with a very close agreement between the models.

The Von Mises equivalent stress contours in Figure 11 show that plastic yielding occurs locally in the Belleville spring section in the flat configuration. This local yielding, which increases with the stroke, contributes to the hysteresis observed both in the experimental test on the spring (Figure 6) and in the experimental test on the converter (Figure 10).

Figure 12 highlights that the flux of the magnetic field originated by the permanent magnet converges on the coils and is only minimally deviated by the steel frame of the elastic conversion system.

By examining the frequency response functions (FRF) in Figure 13, first of all it appears that the experimental resonant frequency of the prototype is completely different (largely higher) than the analytical and numerical predictions and exhibit non-linear effects. Such a difference between theory and practice can be imputed first of all to the two strong simplifying assumptions underlying the analytical model. First, in order to obtain a closed-form solution for the dynamic equation of motion (11), the model neglects the weight load of the system, thus leading to equation (12). However, due to the experimental equipment available in the laboratory, the prototype was set-up and tested along the vertical axis: it comes that the higher its mass, the larger the discrepancy between the experimental and analytical results. Second, the linear behaviour assumption for the elastic system, leading to the fundamental frequency of equation (17), proved to be far from the real response of the Belleville springs (see the experimental dashed curve in Figure 10). On the one hand, the springs stiffness is not zero across the initial equilibrium position; on the other hand, the springs exhibit a significant hysteresis between the loading and unloading cycle. In addition, also the electromechanical coupling affects the system dynamics, but, at this point in the development, its effect was not incorporated in the analytical treatment of the fundamental frequency. According to different authors from the literature [73]-[79], a simple estimate of the electromechanical coupling coefficient for the prototype converter configuration (Figure 7) is given by the following formula:

$$K = N B_r l \tag{19}$$

where N is the number of turns in the coil, B_r is the radial component of the magnetic induction evaluated at the radius of the coil, and l is the circumference of the coil loop. In case of a 1000 loops coil enclosing four magnets (the largest configuration in Figure 13), by retrieving the radial component of the magnetic field from the electromagnetic computational model (Section 5.3), the coupling coefficient K is equal to about 0.3 (N/A). Thus, in the author opinion, electromechanical coupling can be assumed as a second order effect compared to the weight load effect and to the linear assumption

behaviour discussed in the two above points. On the whole, Figure 13 highlights a wide frequency response of the prototype, since the FRF curves show a large peak, in particular in the configurations involving 2 or 4 magnets. This is due to the higher mass of the system that increases the deflection of the bottom Belleville spring, while unloading the top spring. By referring to Figure 10, it comes that the equilibrium configuration of the system displaces leftward and the useful stroke of the device increases. In particular, this gives a bi-stable response of the system between the local maximum on the left and the local minimum on the right (see the dashed experimental curve in Figure 10): over a large frequency range, above a given input acceleration value, the system can jump between these opposite local equilibrium points. It comes a noticeable conversion efficiency of the system.

Figure 14 shows that the proposed harvester provides a significant output voltage in a wide frequency range, in particular for configurations involving 2 or 4 magnets. The output voltage value is nearly the same for both input acceleration levels, but the bandwidth significantly increases doubling the input acceleration. The largest bandwidth, from 120 Hz up to 180 Hz, was registered for the 4 magnets configuration with an input acceleration equal to 2*g* (Figure 14f). This peculiar effect of the input acceleration on the bandwidth of the harvester can be attributed to the bi-stable characteristic exhibited by the harvester itself, as discussed above.

Focusing on the peak resonant frequency of the harvester, from Table 2 it appears that the peak output voltage depends almost linearly from the resistive load and the peak output power from the input acceleration.

A similar observation can be made from Table 3 where the number of magnets and the input acceleration remarkably affects both the peak output voltage and the peak output power. However, these responses reach saturation when both the number of magnets and input acceleration are set to the highest level.

The bar charts in Figure 15 provide a comprehensive summary of Table 2 and Table 3. On the one hand, both the peak output voltage (Figure 15a) and the peak output power (Figure 15b) linearly increase with the number of magnets. On the other hand, the effect of the input acceleration is significant but sub-linear, confirming the saturation of the harvester. In addition, the good agreement between the analytical prediction (dotted bars) and the experimental measurements (solid bars) of the peak output power (Figure 15b) testifies a remarkable energy conversion of the system.

By comparing the performances of this harvester to those existing in the literature for similar techniques, as those reported by Beeby et al. [58], or commercial products like Perpetuum [59], it appears that the proposed harvester:

(i) performs much better in terms of power generation, which is up to two times the higher value reported in [58];

(ii) has a quite large bandwidth, compared to the single resonant frequency of the devices reported in [58];

(iii) needs an input acceleration in the same range as the values reported in [58];

(iv) involves a significantly higher mass and volume than those in [58], but, in the author's opinion, the whole system can be easily scaled down without remarkably affecting the above performances.

As additional observation, compared to non-linear energy harvesters presented in the literature [32]-[55], the proposed solution is quite simple and innovative since it can provide either a linear or a non-linear and bi-stable response, depending on the preload applied to the counteracting Belleville springs.

In conclusion, the proposed energy harvester appears as a promising solution to efficiently harvest ambient energy on a large bandwidth. Further investigations will be performed in order to develop a smaller configuration and also with ad-hoc springs, featuring the ideal zero stiffness response across their flat configuration.

8. CONCLUSIONS

The work proposed and investigated an innovative electromagnetic energy harvesting concept based on two counteracting Belleville springs. By exploiting their peculiarity of an ideally zero stiffness across their flat configuration (for a height to thickness ratio equal to 1.414), a low frequency system can be obtained. The experimental validation of a prototype, involving non-optimal commercial Belleville springs, highlighted a bi-stable characteristic of the harvester and a completely different frequency response. For different resistive loads and input accelerations, the prototype exhibited a remarkably large bandwidth, extending continuously in the range from 120 Hz up to 180 Hz. In this frequency range, all the examined configurations provided a significant output voltage and a remarkable output power, also in comparison with similar literature solutions or commercial electromagnetic harvesters. These encouraging results support further investigations in order to fully exploit the peculiarity of this solution, which can feature either a non-linear or a linear response according to the preload applied to the springs.

REFERENCES

[1] Despesse, G., Jager, T., Chaillout, J.J., Le´ger, J.M., and Basrour, S., 2005, "Design and Fabrication of a New System for Vibration Energy Harvesting", in *Proc. Ph.D. Res. Microelectron. Electron.*, **1**, 225–228.

[2] Luca Gammaitoni, Helios Vocca, Igor Neri, Flavio Travasso and Francesco Orfei (2011). Vibration Energy Harvesting: Linear and Nonlinear Oscillator Approaches, Sustainable Energy Harvesting Technologies - Past, Present and Future, Dr. Yen Kheng Tan (Ed.), ISBN: 978-953-307-438-2.

[3] I. Neri, F. Travasso, R. Mincigrucci, H. Vocca, F. Orfei, L. Gammaitoni, A real vibration database for kinetic energy harvesting application, J. of Intelligent Material Systems and Structures, 2012, 23(18), 2095-2101.

[4] Beeby, S. P., Tudor, M. J., and White, N.M., 2006, "Energy harvesting vibration sources for microsystems applications", *Meas. Sci. Technol.*, **17**, R175–R195.

[5] Dewei, J. and Jing L.,2009, "Human power-based energy harvesting strategies for mobile electronic devices", *Front. Energy Power Eng. China*, **3**(1), 27–46.

[6] A. Khaligh, P. Zeng, and C. Zheng, 2010, "Kinetic energy harvesting using piezoelectric and electromagnetic technologies—state of the art", IEEE Transactions on Industrial Electronics, **57**(3).

[7] T. von Büren, and G. Tröster, 2007, "Design and optimization of a linear vibration-driven electromagnetic micro-power generator", Sensors and Actuators, **A 135**, 765–775.

[8] I. Sari, T. Balkan, and H. Külah, 2010, “An electromagnetic micro power generator for low-frequency environmental vibrations based on the frequency upconversion technique”, J. of Microelectromechanical Systems, **19**(1), 14-27.

[9] A. Z. Trimble, J. H. Lang, J. Pabon, and A. Slocum, 2010, “A Device for Harvesting Energy From Rotational Vibrations”, J. of Mechanical Design, **132**, 091001-1 - 091001-6.

[10] R. Dayal, S. Dwari, and L. Parsa, 2011, “A new design for vibration-based electromagnetic energy harvesting systems using coil inductance of microgenerator”, IEEE Transactions on Industry Applications, **47**(2), 820-830.

[11] C. R. Saha, T. O’Donnell, H. Loder, S. Beeby, and J. Tudor, 2006, “Optimization of an Electromagnetic Energy Harvesting Device”, IEEE Transactions on Magnetics, **42**(10), 3509-3511.

[12] P. Glynne-Jones, M.J. Tudor, Beeby S. P. and White N. M., 2004, “An electromagnetic, vibration-powered generator for intelligent sensor systems”, Sensors Actuators, **A110**, 344–399.

[13] C. B. Williams, C. Shearwood, M. A. Harradine, P. H. Mellor, T. S. Birch and R. B. Yates, 2001, “Development of an electromagnetic micro-generator”, IEE Proc. Circuits Devices Syst., **148**(6), 337-342.

[14] Amirtharajah R. and Chandrakasan A.P., 1998, “Self-powered signal processing using vibration-based power generation”, IEEE J. Solid-State Circuits, 33687–95.

[15] Li W J., Wen Z., Wong P.K., Chan G. M. H. and Leong P H W, 2000, “A micromachined vibration-induced power generator for low power sensors of

robotic systems", Proceedings of World Automation Congress: 8th Int. Symp. on Robotics with Applications (Hawaii).

[16] Ching N. N. H., Wong H. Y., Li W. J., Leong P. H. W. and Wen Z., 2002, "A laser-micromachined vibrational to electrical power transducer for wireless sensing systems", Sensors Actuators, **A97**, 98685–90.

[17] S P Beeby, R N Torah, M J Tudor, P Glynne-Jones, T O'Donnell, CRSaha and S Roy, 2007, "A micro electromagnetic generator for vibration energy harvesting", J. Micromech. Microeng., 17, 1257–1265.

[18] Glynne-Jones, F., Beeby, S.P., and White, N.M., 2001, "Towards a piezoelectric vibration-powered micro-generator", in *IEE Proc. Sci. Mem. Technol.*, **148**(2), 68-72.

[19] S. Zurn, M. Hsieh, G. Smith, D. Markus, M. Zang, G. Hughes, Y. Nam, M. Arik and D. Polla, 2001, "Fabrication and structural characterization of a resonant frequency PZT microcantilever", *Smart Mater. Struct.*, **10**(2), 252-263.

[20] S. Roundy, P.K. Wright, J. Rabaey, 2003, "A study of low level vibrations as a power source for wireless sensor nodes", *Computer Communications*, **26**, 1131–1144.

[21] A. Erturk and D.J. Inman, 2009, "An experimentally validated bimorph cantilever model for piezoelectric energy harvesting from base excitations", *Smart Mater. Struct.*, **18**, 1-18.

[22] Shen, D., Choe, S. Y., and Kim, D. J., 2007, "Analysis of Piezoelectric Materials for Energy Harvesting Devices Under High-g Vibrations", *Jap. J. Appl. Phys.*, **46**(10), 6755–6760.

[23] Benasciutti, D., Moro, L., Zelenika, S., and Brusa, E., 2010, "Vibration energy scavenging via piezoelectric bimorphs of optimized shapes", *Microsyst. Technol.*, **16**, 657–668.

[24] Song, H. J., Choi, Y. T., Wang, G., and Wereley, N. M., "Energy Harvesting Utilizing Single-Crystal PMN-PT Material and Application to a Self-Powered Accelerometer", *J. Mech. Des.*, **131**(9), 091008.

[25] Ferrari, M., Ferrari, V., Guizzetti, M., Marioli, D., and Taroni, A., 2008, "Piezoelectric Multifrequency Energy Converter for Power Harvesting in Autonomous Microsystems", *Sens. Actuators*, **142**, 329–335.

[26] Qi, S., Shuttleworth, R., and Oyadiji, S. O., 2009, "Multiple Resonances Piezoelectric Energy Harvesting Generator", in *Proceedings of SMASIS*, CA.

[27] Shahruz, S. M., 2006, "Design of Mechanical Band-Pass Filters for Energy Scavenging: Multi-Degree-of-Freedom Models", *Mechatronics*, **16**, 523–531.

[28] D. Benasciutti, L. Moro e M. Gallina, "On the optimal bending deflection of piezoelectric scavengers", J. of Intelligent Material Systems and Structures, **24**(5), 627-639, 2013.

[29] D. Castagnetti, 2011, "Fractal-Inspired Multi-Frequency Structures for Piezoelectric Harvesting of Ambient Kinetic Energy", *J. of Mech. Design*, **133**(11), 111005-1 - 111005-8.

[30] D. Castagnetti, 2012, "Experimental modal analysis of fractal-inspired multi-frequency piezoelectric energy converters", *Smart Mater. Struct.*, **21**, 1-9.

[31] D. Castagnetti (2013), "A wideband fractal-inspired piezoelectric energy converter: design, simulation and experimental characterization", *Smart Materials and Structures*, 22, 1-11, 094024.

[32] Daqaq, M. F., 2010, "Response of uni-modal duffing-type harvesters to random forced excitations", *Journal of Sound and Vibration*, **329**, 3621-3631.

[33] Bibo, A., Li, G., Daqaq, M. F., 2011, "Electromechanical Modeling and Normal Form Analysis of an Aeroelastic Micro-Power Generator", *J. of Intelligent Material Systems and Structures*, **22**(6), 577-592.

[34] Bryant, M., Garcia, E., 2011, "Modeling and testing of a novel aeroelastic flutter energy harvester", *Journal of Vibrations & Acoustics*, **133**, 12.1–12.11.

[35] Singh, K., Michelin, S., and de Langre, E., 2012, "Energy harvesting from axial fluid-elastic instabilities of a cylinder", *J. of Fluids and Structures*, **30**, 159-172.

[36] Burrow, S. G., Clare, L. R., Carrella, A., Barton, D., Vibration energy harvesters with non-linear compliance, *Proceedings of SPIE* 6928 (2008) 692807.

[37] Mann, B. P., Sims, N. D., Energy harvesting from the non linear oscillations of magnetic levitation, *Journal of Sound and Vibration*, 319 (2009)515–530.

[38] Ramlan, R. , Brennan, M. J., Mace, B. R.,Kovacic, I., 2009, Potential benefits of a non-linear stiffness in an energy harvesting device, *Nonlinear Dynamics*, 59, 545–558.

[39] Daqaq, M. F., 2010, Response of uni-modal Duffing-type harvesters to random forced excitations, *Journal of Sound and Vibration*, 329, 3621–3631.

[40] Stanton, S. C., Mc Gehee, C. C., and Mann, B. P., Reversible hysteresis for broad band magnetopiezoelastic energy harvesting, Applied Physics Letters 96 (2010) 174103.

[41] Gammaitoni, L.,Neri, I., and Vocca H., 2009, "Nonlinear oscillators for vibration energy harvesting", *Applied Physics Letters*, 94, 164102.

[42] Lee, C., Stamp, D., Kapania, N., and Mur-Miranda, J.O., 2010, "Harvesting Vibration Energy Using Nonlinear Oscillations of an Electromagnetic Inductor", *Proc. of SPIE*, **7683**, 76830Y.

[43] Erturk, E., and Inman, D., 2011, "Broadband piezoelectric power generation on high-energy orbits of the bistable Duffing oscillator with electromechanical coupling", Journal of Sound and Vibration, **330**, 2339–2353.

[44] Sebald, G., Kuwano, H., Guyomar, D., and Ducharne, B., 2011 "Experimental Duffing oscillator for broadband piezoelectric energy harvesting", *Smart Mater. Struct.*, **20**, 102001.

[45] Cottone, F. Basset, P., Vocca, H., and Gammaitoni, L., 2012, "Electromagnetic buckled beam oscillator for enhanced vibration energy harvesting", *Proc. Of the 2012 IEEE International Conference on Green Computing and Communications, Conference on Internet of Things, and Conference on Cyber, Physical and Social Computing*, 624-927.

[46] Liu, H., Lee, C., Kobayashi, T., Tay, C. J., and Quan, C., 2012, "Investigation of a MEMS piezoelectric energy harvester system with a frequency-widened-bandwidth mechanism introduced by mechanical stoppers", *Smart Mater. Struct.*, **21**, 035005.

[47] Pellegrini, S. P., Tolou, N., Schenk, M., and Herder, J. L., Bistable vibration energy harvesters: A review, *Journal of Intelligent Material Systems and Structures*, **24**(11), 1303–1312.

[48] Harne, R. L., and Wang, K. W., 2013, "A review of the recent research on vibration energy harvesting via bistable systems, *Smart Materials and Structures*, **22**, 023001.

[49] Jianga, W. A., and Chen, L. Q., 2013, "Energy harvesting of monostable Duffing oscillator under Gaussianwhite noise excitation", Mechanics Research Communications 53, 85– 91.

[50] Zhao, S., and Erturk A., 2013, "On the stochastic excitation of monostable and bistable electroelastic power generators: Relative advantages and tradeoffs in a physical system", APPLIED PHYSICS LETTERS 102, 103902

[51] Brzeski, P., Perlikowski, P., Kapitaniak T., 2014, Numerical optimization of tuned mass absorbers attached to strongly nonlinear Duffing oscillator, *Commun Nonlinear Sci Numer Simulat,* **19**, 298–310.

[52] Su, D., Nakano, K., Zheng, R., and Cartmell, M.P., 2014, "On electrical optimisation using a Duffing-type vibrational energy harvester", *Proc IMechE Part C: J Mechanical Engineering Science*, 1-12.

[53] Leadenham, S., and Erturk, A., 2014, "M-shaped asymmetric non linear oscillator for broadband vibration energy harvesting: Harmonic balance analysis and experimental validation", *Journal of Sound and Vibration*, **333**, 6209–6223.

[54] Suhaimi, K., Ramlan, R., and Putra, A., 2014, "A Combined Softening and Hardening Mechanism for Low Frequency Human Motion Energy Harvesting Application", *Advances in Acoustics and Vibration*, 1-13,

[55] Xia, H., and Chen, R., 2014, "Design and analysis of a scalable harvesting interface for multi-sourcepiezoelectric energy harvesting", *Sensors and Actuators*, A 218 33–40.

[56] Challa, V.R., Prasad, M. G., and Fisher, F.T., 2009, "A coupled piezoelectric–electromagnetic energy harvesting technique for achieving increased power output through damping matching", Smart Mater. Struct., **18**, 095029.

[57] Khaligh, A., Zeng, P., Wu, X., and Xu, Y., 2008, "A hybrid energy scavenging topology for human-powered mobile electronics", Industrial Electronics, 2008. IECON 2008. 34th Annual Conference of IEEE, 448-453.

[58] Beeby, S. P., Tudor, M. J., and White, N. M., 2006, "Energy harvesting vibration sources for microsystems applications", *Meas. Sci. Technol.*, 17, R175-R195.

[59] www.perpetuum.co.uk

[60] Bagavathiperumal, P., Chandrasekaran, K., and Manivasagam, S., 1991, "Elastic load-displacement predictions for coned disc springs subjected to axial loading using the finite element method", *J. of Strain Analysis*, 26(3), 147-152.

[61] Mubea disc spring handbook, 2012, (available at: http://www.mubea.com/uploads/media/Mubea_Disc_Springs_Manual_01.pdf).

[62] Almen, J. O., and Laszlo, A., 1936, "The uniform section disk spring", *Trans. of the ASME*, 58, 305-314.

[63] Meirovitch, L., "Fundamentals of vibrations", *McGrawHill*, Singapore, 1 ed. 2001.

[64] Nayfeh, A. H., 1993, Introduction to perturbation techniques, Wiley-VCH, 1st ed., New York, USA.

[65] Williams, C. B., and Yates, R. B., "Analysis of a micro-electric generator for microsystems", *Sensors Actuators A*, 52, 8–11, 1996.

[66] www.supermagnete.it

[67] Finite Element Method Magnetics Version 4.2 User's Manual, http://www.femm.info/wiki/Documentation/

[68] SimuliaABAQUS6.12-3,Users' manual. Providence, RI, USA: HKS Inc.,2012.

[69] www.dataphysics.com/

[70] TDS Miniature Accelerometers on www.mmf.de

[71] www.ni.com/products/

[72] www.ni.com/labview/

[73] Cannarella, J., Selvaggi, J., Salon, S., Tichy, J., and Borca-Tasciuc, D. A., 2011, "Coupling Factor Between the Magnetic and Mechanical Energy Domains in Electromagnetic Power Harvesting Applications", *IEEE Transactions on Magnetics*, 47(8), 2076-2080.

[74] Beeby, S. P., Torah, R. N., Tudor, M. J., Glynne-Jones, P., O'Donnell, T., Saha, C. R., and Roy, S., 2007, "A micro electromagnetic generator for vibration energy harvesting", *J. Micromech. Microeng.*, 17, 1257–1265.

[75] Williams, C. B., and Yates, R. B., 1996, "Analysis of a micro-electric generator for microsystems", *Sens. Actuators*, 52, 8–11.

[76] Amirtharajah, R., and Chandrakasan, A.P., 1998, “Self-powered signal processing using vibration-based power generation”, *IEEE J. Solid State Circuits*, 33(5), 687–695.

[77] Roundy, S., Wright, P. K., and Rabaey, J. M., 2004, “Energy Scavenging for Wireless Sensor Networks With Special Focus on Vibrations”, *Norwell,* MA: Kluwer.

[78] Stephen, N. G., 2006, “On energy harvesting from ambient vibration,” *J. Sound Vib.*, 293, 409–425.

[79] El-hami, M., Glynne-Jones, P., White, N. M., Hill, M., Beeby, S., James, E., Brown, A. D., and Ross, J. N., 2001, “Design and fabrication of a new vibration-based electromechanical power generator,” *Sens. Actuators A*, 92, 335–342.

FIGURES AND TABLES

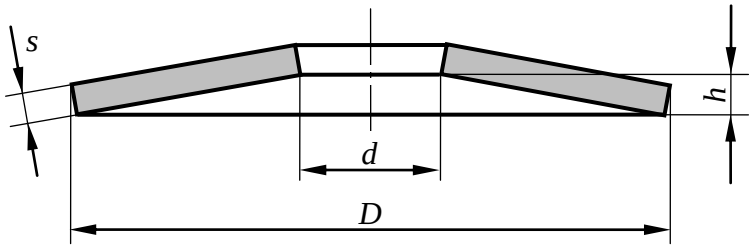

Figure 1 Section view of a Belleville spring.

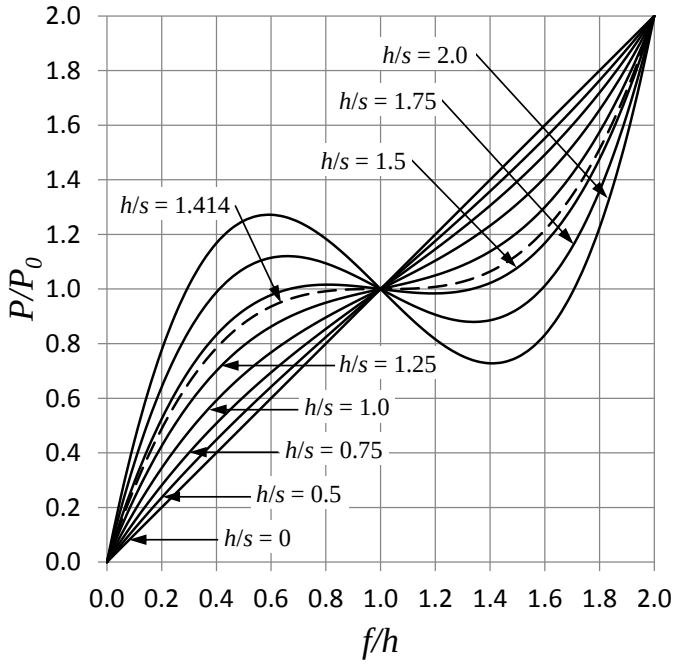

Figure 2 Dimensionless force-deflection curves for height to thickness ratios from 0 to 2.

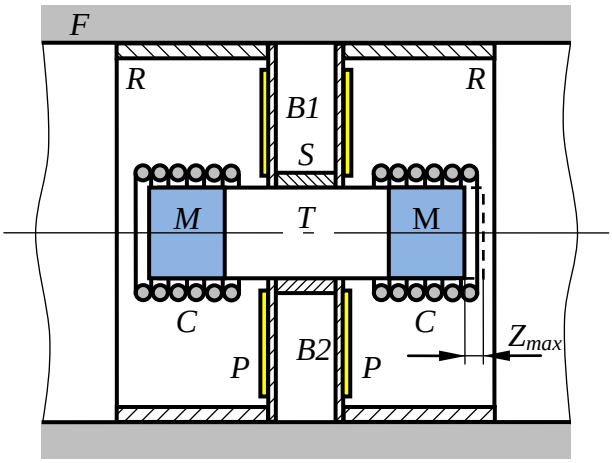

Figure 3 Conceptual solution for an energy harvester.

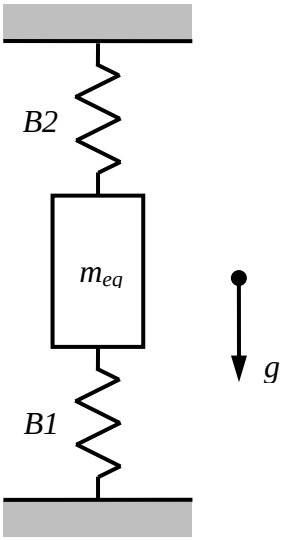

Figure 4 Equivalent mass-spring model of the elastic system.

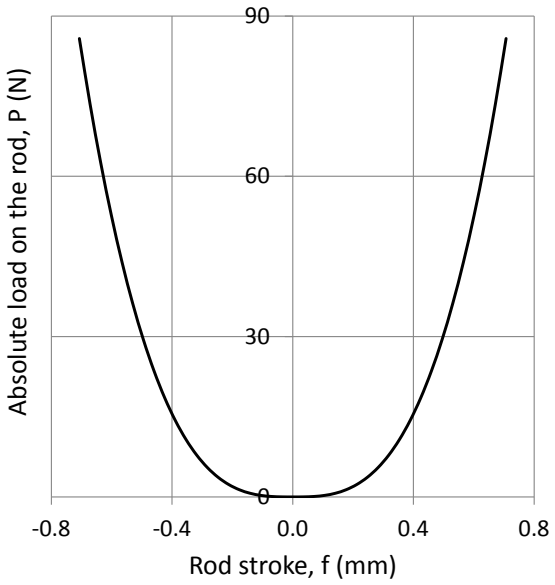

Figure 5 Absolute load on the rod versus rod stroke as provided by the analytical model.

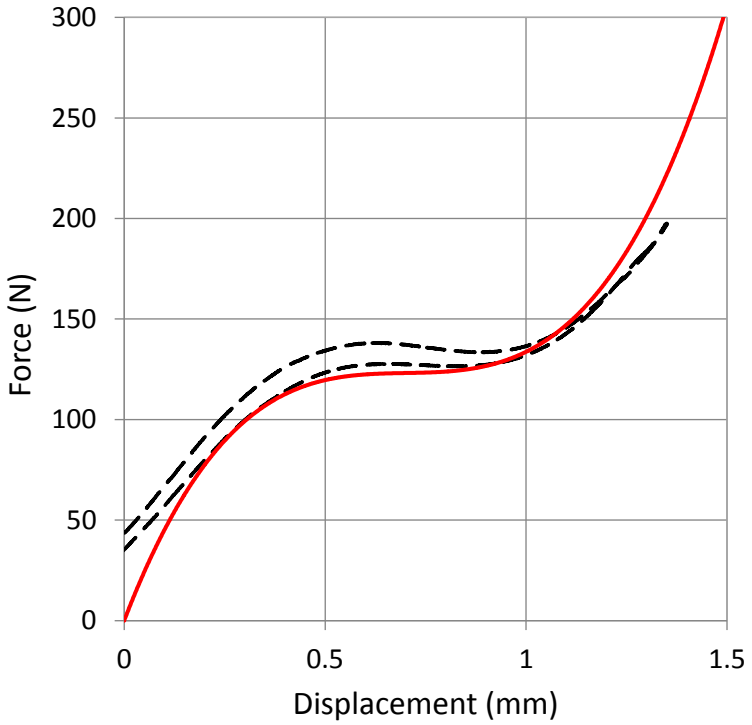

Figure 6 Analytical (solid line) and experimental (dashed line) force-displacement response of the Belleville spring # 1 in Table 1.

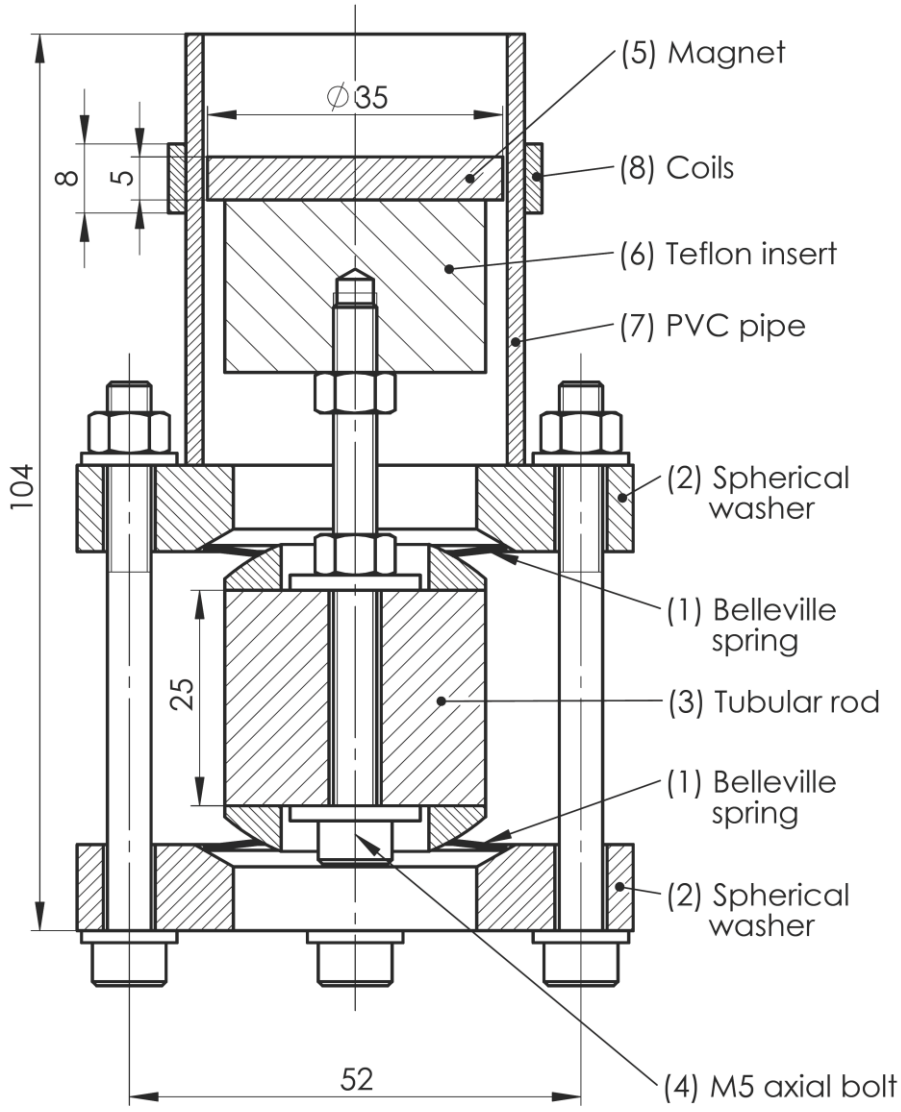

Figure 7 Technical drawing of the harvester prototype.

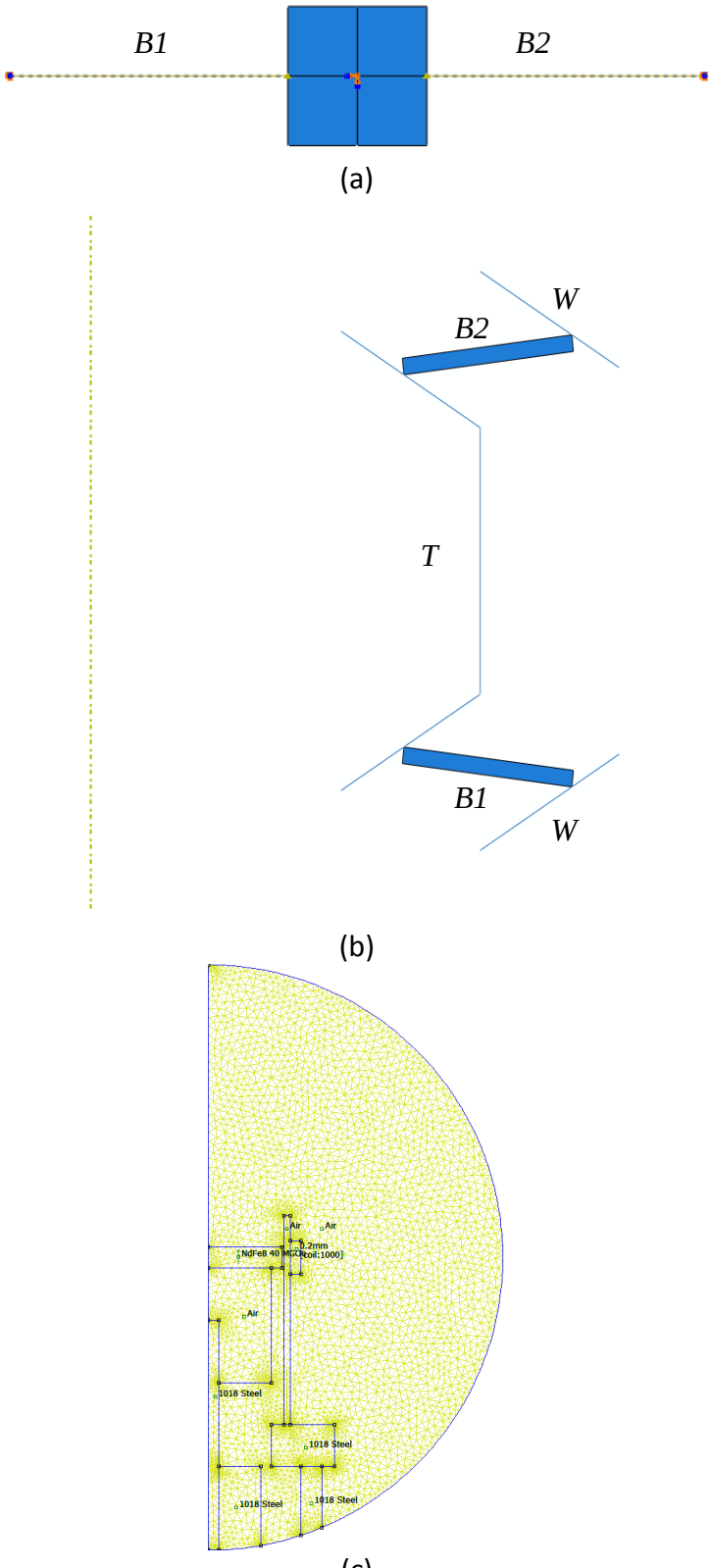

Figure 8 Mass-spring (a), axisymmetric structural (b) and axisymmetric magnetostatic (c) FE model of the harvester prototype.

Figure 9 Harvester prototype on the vibrating table

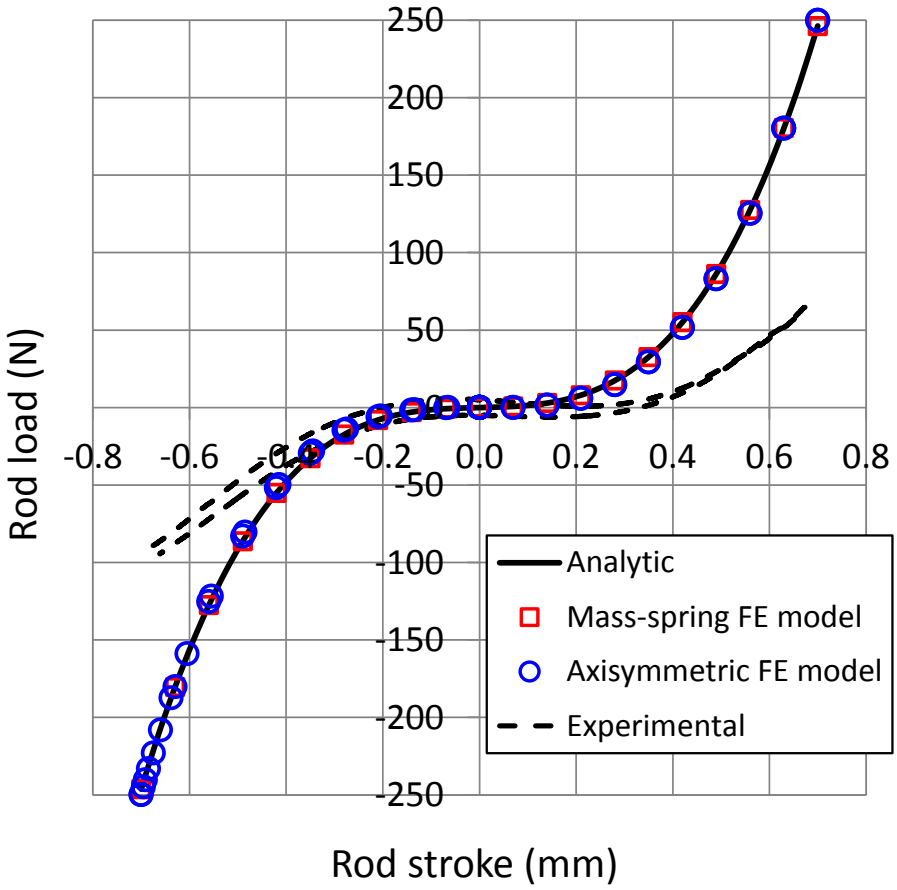

Figure 10 Load-stroke curves of the rod (T) as provided by the analytical model, FE model, and experimental tests.

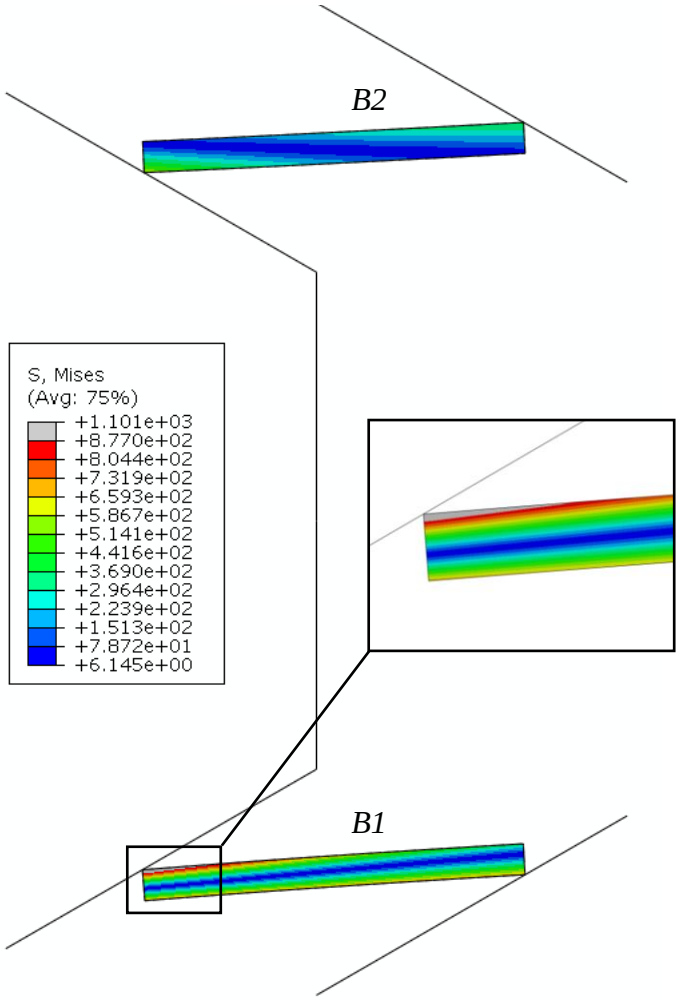

Figure 11 Von Mises equivalent stress on the Belleville springs, beyond their flat configuration.

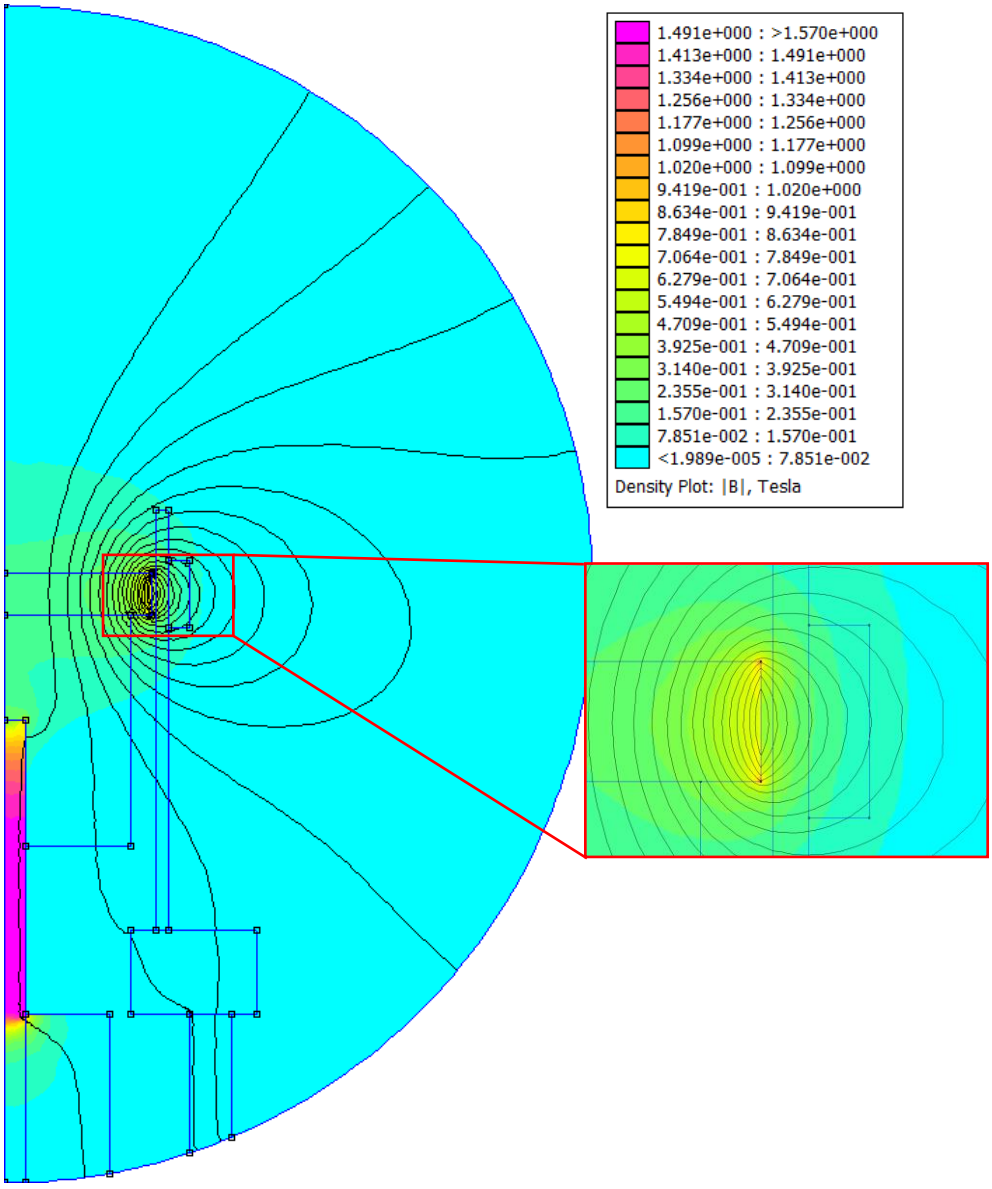

Figure 12 Flux of the magnetic field B in the converter, with a close up view of. the interaction between the permanent magnet and the coil.

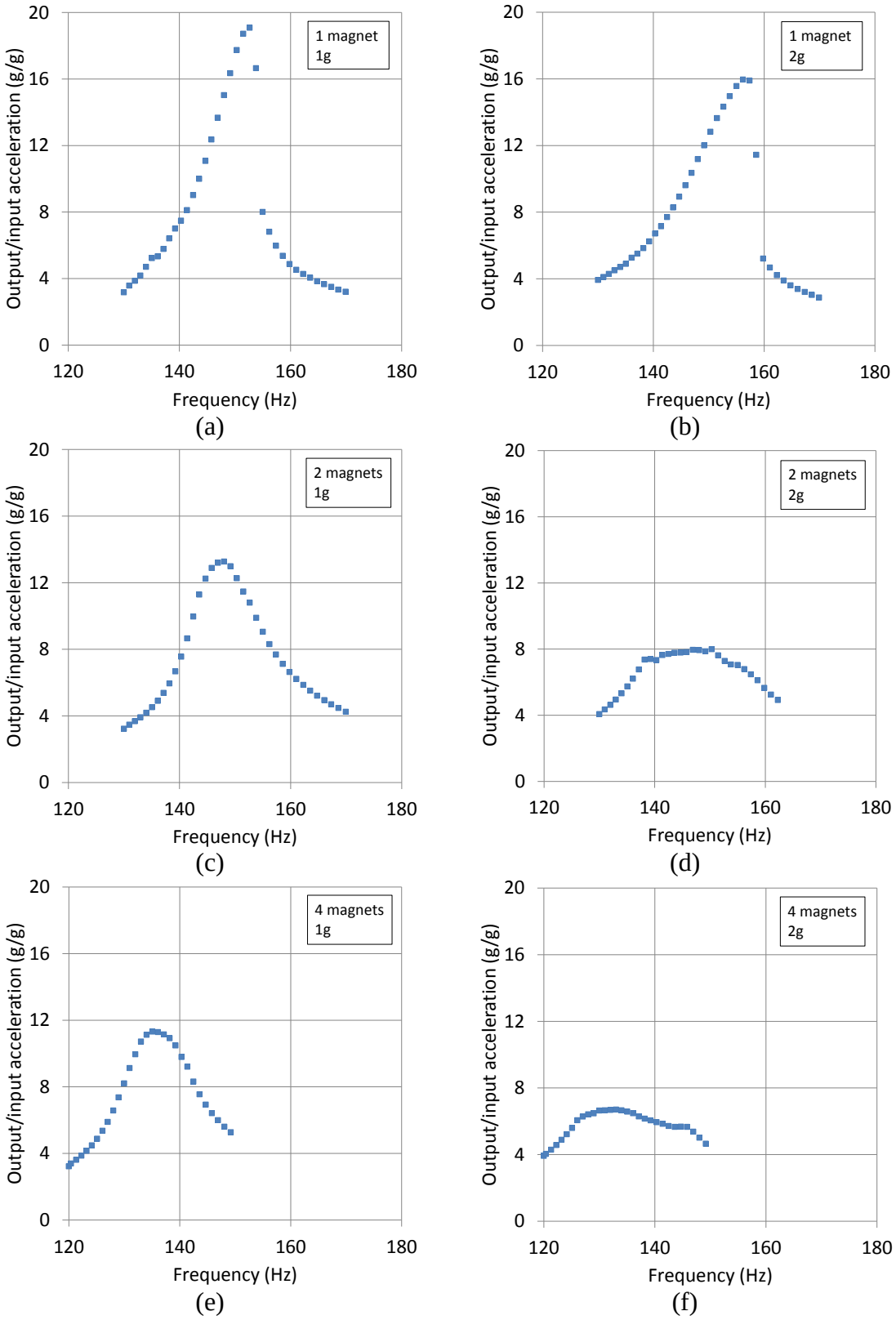

Figure 13 Ratio of the output acceleration on the moving mass over the input acceleration on the frame as a function of the exciting frequency for a 100 Ω resistive load.

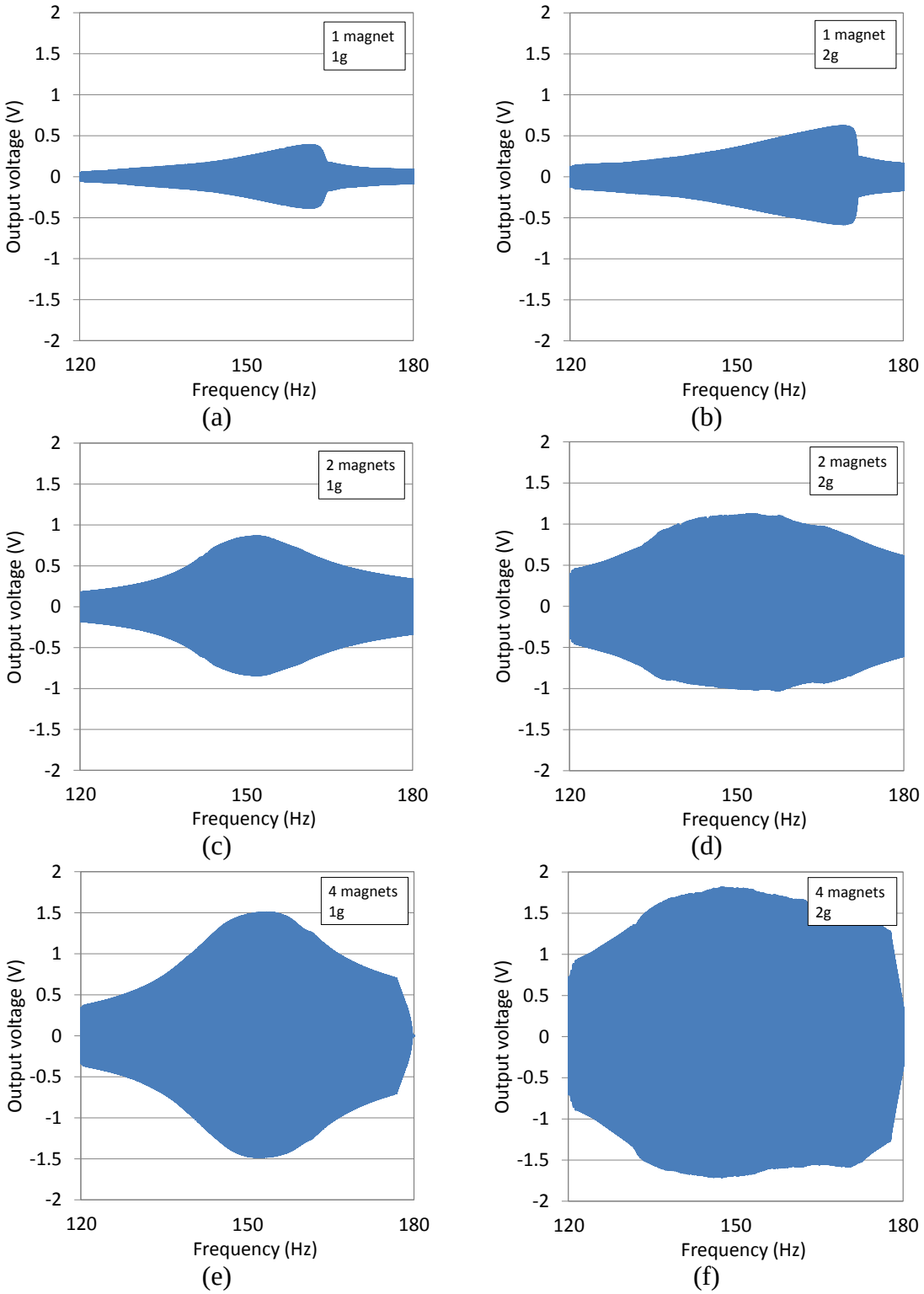

Figure 14 Output voltage from the converter as a function of the exciting frequency for a 100 Ω resistive load.

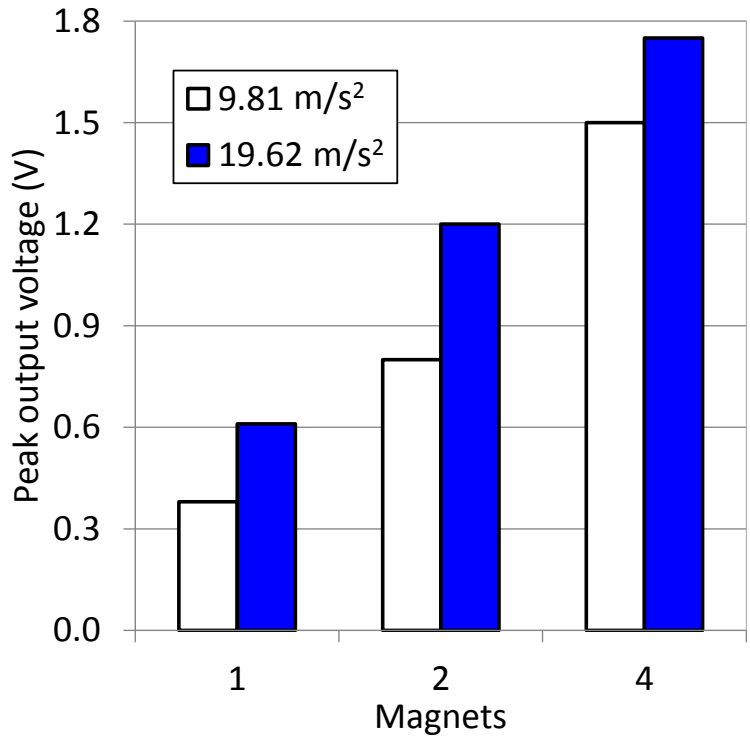

(a)

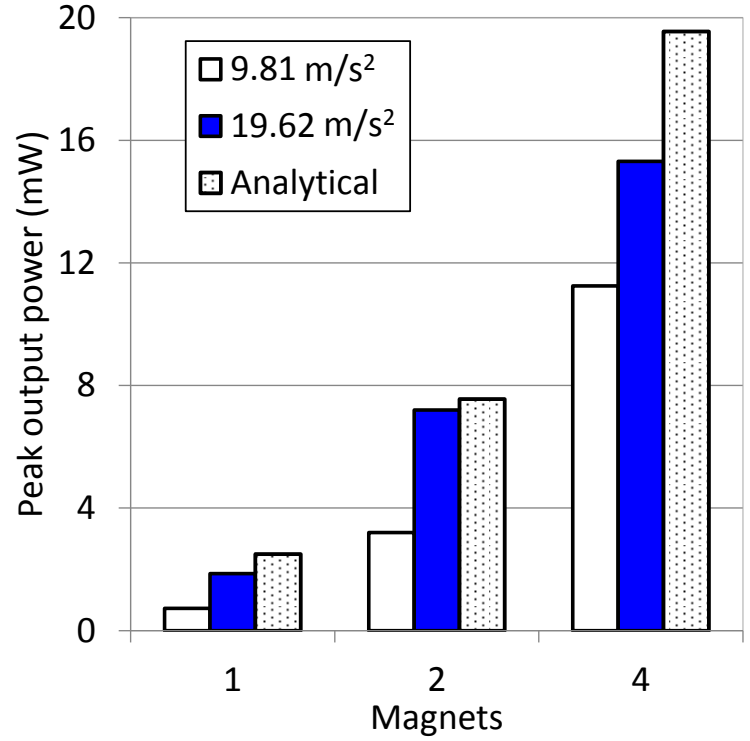

(b)

Figure 15 Peak output voltage (a) and peak output power (b) at resonant frequency with a 100 Ω resistive load.

Table 1 Dimensions of selected commercial Belleville springs

#	Outer diameter, D (mm)	Inner diameter, d (mm)	Heigth, h (mm)	Thickness, s (mm)	h/s
1	34.6	22.4	0.70	0.50	1.400
2	67.5	50.5	1.00	0.70	1.428

Table 2 Peak output voltage and peak output power for the energy harvester with 1 magnet

Input acceleration	9.81 m/s^2		19.62 m/s^2	
Resistive load	Peak output voltage (V)	Peak output power (mW)	Peak output voltage (V)	Peak output power (mW)
Open circuit	0.78	--	0.80	--
180 Ω	0.50	0.694	0.75	1.563
100 Ω	0.38	0.722	0.61	1.860
82 Ω	0.30	0.549	0.55	1.844
68 Ω	0.22	0.356	0.43	1.360

Table 3 Peak output voltage and peak output power for the energy harvester with 2 and 4 magnets and a 100 Ω resistive load.

Input acceleration	9.81 m/s^2		19.62 m/s^2	
n.° of magnets	Peak output voltage (V)	Peak output power (mW)	Peak output voltage (V)	Peak output power (mW)
2	0.8	3.2	1.2	7.2
4	1.5	11.25	1.75	15.31